Crystal Structures, Mössbauer Spectra and Magnetic Properties of Two Iron(III) Spin-crossover Complexes†

Yonezo Maeda,*[a] Hiroki Oshio,[b] Koshiro Toriumi[b] and Yoshimasa Takashima[b]

[a] *Department of Chemistry, Faculty of Science, Kyushu University, Hakozaki, Higashiku, Fukuoka 812, Japan*

[b] *Institute for Molecular Science, Okazaki, Aichi 444, Japan*

The six-co-ordinate iron(III) complexes $[Fe(bzpa)_2]ClO_4$ (Hbzpa = (1-benzoylpropen-2-yl)(2-pyridylmethyl)amine] and $[Fe(acen)(NC_5H_3Me_2\text{-}3,4)_2]BPh_4$[$H_2$acen = ethylenebis(acetylacetoneiminate)] have been shown by variable-temperature magnetic and Mössbauer spectroscopy measurements to be spin-crossover ($S = \frac{5}{2} \rightleftharpoons S = \frac{1}{2}$) complexes. Magnetic moments for both complexes show a continuous variation with temperature, which parallels that of the absorption area under the Mössbauer spectra. 'Time-averaged' Mössbauer spectra between the high- and low-spin states were observed for $[Fe(bzpa)_2]ClO_4$. X-Ray crystallographic structure determinations for both complexes were done for both high- and low-spin states. Both cations possess a N_4O_2 donor-atom set forming a distorted octahedron about the metal atom, and the terminal oxygen donor atoms occupy *cis* positions. The average metal–ligand bond lengths for the low-spin form are shorter by 0.069 Å for the bzpa complex and 0.104 Å for the acen complex than for the appropriate high-spin form. Remarkable changes in the Fe–O–C angles for both complexes are observed with spin-state transformation. In $[Fe(acen)(NC_5H_3Me_2\text{-}3,4)_2]BPh_4$ the two axial positions are occupied by the nitrogen atom of the 3,4-dimethylpyridine ligand. Crystal data: $[Fe(bzpa)_2]ClO_4$, space group $I4_1/a$, $Z = 16$ $\alpha = \beta = \gamma = 90.00°$, (at 290 K) $a = b = 27.965(6)$, $c = 15.525(4)$ Å, $R = 0.050$, 3550 reflections, (140 K) $a = b = 27.456(9)$, $c = 15.400(4)$ Å, $R = 0.044$, 3236 reflections; $[Fe(acen)(NC_5H_3Me_2\text{-}3,4)_2]BPh_4$ space group $P2_1/a$, $Z = 4$, $\alpha = \gamma = 90.00°$, $a = 28.021(3)$ (at 298 K), $b = 14.313(2)$, $c = 11.166(1)$ Å, $\beta = 90.68(1)°$, $R = 0.038$, 3546 reflections, (at 120 K) $a = 27.707(4)$, $b = 14.085(2)$, $c = 10.998(2)$ Å, $\beta = 91.04(1)°$, $R = 0.037$, 5906 reflections. The results support a model in which flexibility of the angle Fe–O–C in the co-ordination sphere is important for change in iron-donor atom bond lengths upon spin-state interexchange.

'Spin-crossover' phenomena of iron(III)[1–7] and -(II)[8–11] complexes have been well studied. In the solid state, the complexes can be classified for convenience into those of the 'gradual transformation type' (g.t.t.) or 'abrupt transformation type' (a.t.t.) on the basis of the temperature dependence of magnetic susceptibilities. Magnetic moments of the complexes in the former type change continuously over a wide temperature range owing to the fact that the spin-state transformation in the complexes proceeds gradually with temperature, or that the electronic spin state of an iron ion is in thermal equilibrium between ^2T ground and ^6A excited states and the equilibrium population is dependent on temperature. The spin-crossover complexes are sensitive not only to temperature, but also to pressure, slight chemical modifications, 'solid-state effects', changes of counter ion or ligand substituent.[12,13] A decrease in bond length for low- relative to high-spin complexes results in a decrease in volume by 5–6 $cm^3\ mol^{-1}$.[14]

The spin-state transformation for the a.t.t. complex $[Fe(phen)_2(NCS)_2]$ (phen = 1,10-phenanthroline) has been interpreted using a domain model[15,16] and the g.t.t. complex $[Fe(acpa)_2]PF_6$ [Hacpa = (1-acetylpropen-2-yl)(2-pyridylmethyl)amine] has a small domain.[17] The importance of lattice distortion around an iron atom,[18,19] lattice expansion[20] and radiationless transition[21] has been pointed out.

Fast spin-state interexchange has been found to occur in iron Schiff-base complexes,[12,22,23] [Fe(salen)(Him)$_2$]Y [salen = ethylenebis(salicylideneiminate), Him = imidazole][24,25] and $[Fe(oep)(NC_5H_4Cl\text{-}3)_2]ClO_4$ (oep = 2,3,7,8,12,13,17,18-octaethylporphyrinate).[26] The spin-crossover behaviour of $[Fe(acen)(NC_5H_3Me_2\text{-}3,4)_2]BPh_4$ [acen = ethylenebis(acetylacetoneiminate)] has been reported elsewhere[13] and the spin-state interexchange rate is slower than the reciprocal of the Mössbauer lifetime. The complexes $[Fe(acpa)_2]PF_6$ and $[Fe(bzpa)_2]ClO_4$ [Hbzpa = (1-benzoylpropen-2-yl)(2-pyridylmethyl)amine] show spin-state interexchange of the same magnitude as the reciprocal of the Mössbauer lifetime.

In the present study, X-ray crystal structure determinations of the complexes $[Fe(bzpa)_2]ClO_4$ and $[Fe(acen)(NC_5H_3Me_2\text{-}3,4)_2]BPh_4$ have been done to ascertain which structural features, if any, influence the nature and dynamics of the spin-state interexchange.

Experimental

The bzpa complex was prepared as described elsewhere[27] and single crystals were obtained from a nearly saturated solution in methanol, evaporated slowly at room temperature. The single crystals of the acen complex were prepared in dichloromethane solution by a similar method. Samples in the same vessels used for preparing the single crystals were subjected to magnetic susceptibility and Mössbauer spectroscopic measurement at various temperatures (78–320 K), except for the sample used for determining the magnetic susceptibility of $[Fe(acen)(NC_5H_3Me_2\text{-}3,4)_2]BPh_4$. Magnetic susceptibility data were obtained by the Faraday method, using an instrument described elsewhere,[27] and $HgCo(NCS)_4$ as a calibrant, and corrected for the diamagnetism of the ligands and anions. The effective magnetic moments were calculated by the formula $\mu_{eff} = 2.83$

† *Supplementary data available* (No. SUP 56810, 4 pp.): plot of equilibrium constant against temperature. See Instructions for Authors, *J. Chem. Soc., Dalton Trans.*, 1991, Issue 1, pp. xviii–xxii.

Table 1 Crystallographic data for $[Fe(bzpa)_2]ClO_4$ and $[Fe(acen)(NC_5H_3Me_2\text{-}3,4)_2]BPh_4$

	$[Fe(bzpa)_2]ClO_4$		$[Fe(acen)(NC_5H_3Me_2\text{-}3,4)_2]BPh_4$	
Formula	$C_{32}H_{30}ClFeN_4O_6$		$C_{50}H_{56}BFeN_4O_2$	
M	657.91		811.67	
T/K	290	140	290	120
Crystal system	Tetragonal	Tetragonal	Monoclinic	Monoclinic
Space group	$I4_1/a$	$I4_1/a$	$P2_1/a$	$P2_1/a$
a/Å	27.965(6)	27.456(9)	28.021(3)	27.707(4)
b/Å			14.313(2)	14.085(2)
c/Å	15.525(4)	15.400(4)	11.166(1)	10.998(2)
β/°			90.68(1)	91.04(1)
U/Å^3	12 140(5)	11 608(5)	4 478(1)	4 291(1)
Z	16	16	4	4
D_c/g cm^{-3}	1.440	1.506	1.204	1.256
D_m/g cm^{-3}	1.45		1.19	
μ(Mo-Kα)/cm^{-1}	6.530	6.829	3.924	4.095
Independent data	3550	3236	3546	5906
R	0.050	0.044	0.038	0.037
R'	0.061	0.043	0.046	0.046

$R = \Sigma(|F_o| - |F_c|)/\Sigma|F_o|$, $R' = [\Sigma w(|F_o| - |F_c|)^2/\Sigma w|F_o|^2]^{\frac{1}{2}}$, where $w = 1/\sigma^2(|F_o|)$.

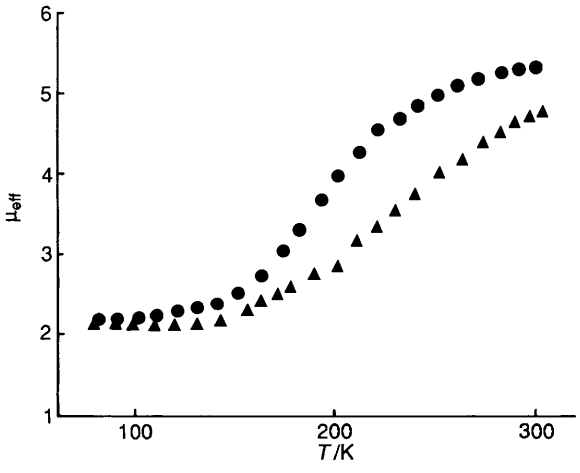

Fig. 1 Temperature dependences of the magnetic moments for $[Fe(bzpa)_2]ClO_4$(▲) and $[Fe(acen)(NC_5H_3Me_2\text{-}3,4)_2]BPh_4$(●)

$(\chi_M T)^{\frac{1}{2}}$, χ_M being a corrected molar magnetic susceptibility and T the temperature in K.

Mössbauer spectra were recorded on equipment previously described using iron foil as a calibrant. All isomer shifts are reported with respect to the centroid of the spectrum of iron foil enriched with ^{57}Fe at 295 K. All spectra were fitted by Lorentzian line shapes using a least-squares method at the Computer Center, Kyushu University.

The relaxation fits were based on the method reported[28] for relaxation between two quadrupole-split doublets representing the low- and high-spin electronic states. The quadrupole splittings of the low- and high-spin doublets in these fits were kept constant at 1.398 and 0.500 mm s^{-1} respectively. The high- and low-spin populations determined from the magnetic data were used. Values of μ_{eff} 2.09 and 5.60 were employed for the low- and high-spin electronic configurations, respectively. The linewidth for the doublet was varied according to the high- or low-spin fraction because keeping the linewidth of the doublet constant resulted in an unreasonable relaxation time and incorrect enthalpy change. The iron atoms in the complexes are surrounded with bulky ligands and therefore the full widths at half maximum for the high-spin isomers at high temperature become broad for spin–spin or spin–lattice relaxation.

X-Ray Crystallography.—Data collection and processing. A crystal was attached to the end of a glass fibre and mounted on a Rigaku AFC-5R four-circle diffractometer; ω–2θ scans were used. Crystallographic data are summarized in Table 1. Intensity data were obtained by using graphite-monochromated Mo-Kα radiation (λ = 0.71073 Å) and those for all non-equivalent reflections having $|F_o| > 3\sigma(F_o)$ were used for processing. The intensities were corrected for Lorentz polarization but not for extinction. Lattice constants were determined by least-squares refinement. The intensities of four standard reflections were monitored every 100 reflections and showed no greater fluctuations during the data collection than those expected from Poisson statistics.

Structure analysis and refinement. The structure was solved by the conventional heavy-atom method and refined by block-diagonal least-squares with anisotropic thermal parameters for non-H atoms and isotropic ones for H atoms. Atomic scattering factors and anomalous scattering coefficients were taken from ref. 29. A weighting scheme of the form $w = [\sigma_c^2 + (0.015|F_o|)^2]^{-1}$ was used where σ_c^2 was the standard deviation of $|F_o|$ calculated from counting statistics.

All calculations were carried out using the program systems UNICS III[30] and ORTEP[31] on a HITAC M680 Hitachi computer at the Computer Centre of the Institute for Molecular Science. Final atom coordinates for the non-hydrogen atoms of $[Fe(bzpa)_2]ClO_4$ and $[Fe(acen)(NC_5H_3Me_2\text{-}3,4)_2]BPh_4$ are given in Tables 2 and 3, respectively.

Additional material available from the Cambridge Crystallographic Data Centre comprises H-atom coordinates, thermal parameters and remaining bond lengths and angles.

Results and Discussion

Magnetic Susceptibility.—The values of the magnetic moments for both complexes obtained in the warming-up mode are plotted in Fig. 1. The magnetic data indicate anomalous behaviour characteristic of a $^6A_1 \rightleftharpoons {}^2T_2$ spin-equilibrium process where the transition occurs continuously with temperature. The values for $[Fe(bzpa)_2]ClO_4$ at low temperature are characteristic of low-spin iron(III) complexes; the values at high temperature are not so large as for typical high-spin complexes, but this behaviour is sometimes observed for spin-crossover complexes.

The magnetic behaviour for freshly prepared $[Fe(acen)(NC_5H_3Me_2\text{-}3,4)_2]BPh_4$ is similar to that previously reported and the transition occurs continuously with temperature.

Mössbauer Spectra.—The ^{57}Fe Mössbauer spectra for the bzpa complex was measured at various temperatures to

Table 2 Positional parameters for $[Fe(bzpa)_2]ClO_4$*

	At 290 K			At 140 K		
Atom	*x*	*y*	*z*	*x*	*y*	*z*
Fe	0.345 47(2)	0.376 42(2)	0.137 02(4)	0.346 45(2)	0.124 40(2)	0.138 96(4)
O(1)	0.383 1(1)	0.433 5(1)	0.137 5(2)	0.386 5(1)	0.068 2(1)	0.143 1(2)
O(2)	0.315 9(1)	0.387 7(1)	0.247 5(2)	0.314 1(1)	0.107 2(1)	0.245 1(2)
N(1)	0.295 4(1)	0.322 7(1)	0.120 7(2)	0.299 7(1)	0.178 4(1)	0.132 3(2)
N(2)	0.293 2(1)	0.412 4(1)	0.075 4(2)	0.296 1(1)	0.090 5(1)	0.078 0(2)
N(3)	0.383 2(1)	0.352 8(1)	0.029 8(2)	0.382 2(1)	0.145 7(1)	0.033 3(2)
N(4)	0.399 2(1)	0.340 6(1)	0.194 6(2)	0.398 6(1)	0.158 1(1)	0.197 2(2)
C(1)	0.302 6(2)	0.276 2(2)	0.135 8(4)	0.309 7(2)	0.226 0(2)	0.146 2(3)
C(2)	0.265 4(2)	0.244 7(2)	0.139 4(5)	0.272 6(2)	0.259 9(2)	0.147 2(3)
C(3)	0.219 7(3)	0.261 1(2)	0.129 9(5)	0.225 2(2)	0.245 7(2)	0.134 7(3)
C(4)	0.212 1(2)	0.308 9(2)	0.113 2(4)	0.215 2(2)	0.196 7(2)	0.119 6(3)
C(5)	0.251 1(2)	0.338 7(2)	0.107 2(3)	0.253 8(1)	0.164 2(1)	0.116 2(3)
C(6)	0.245 4(2)	0.390 6(2)	0.085 4(3)	0.247 5(1)	0.111 7(2)	0.092 0(3)
C(7)	0.297 8(2)	0.453 1(2)	0.034 9(3)	0.301 1(1)	0.049 2(1)	0.035 3(2)
C(8)	0.342 2(2)	0.477 9(2)	0.033 8(3)	0.346 3(2)	0.024 5(1)	0.032 8(3)
C(9)	0.381 5(2)	0.468 9(2)	0.083 1(3)	0.385 5(1)	0.032 9(1)	0.087 4(3)
C(10)	0.424 1(2)	0.500 4(2)	0.084 1(3)	0.429 5(1)	0.001 1(1)	0.088 5(3)
C(11)	0.459 9(2)	0.491 7(2)	0.144 7(4)	0.438 3(2)	−0.035 3(2)	0.027 1(3)
C(12)	0.501 2(2)	0.518 5(2)	0.148 3(4)	0.480 3(2)	−0.062 6(2)	0.030 4(3)
C(13)	0.507 4(2)	0.554 5(2)	0.088 7(5)	0.514 3(2)	−0.054 9(2)	0.094 6(3)
C(14)	0.473 6(2)	0.563 3(2)	0.028 2(4)	0.506 1(2)	−0.020 1(2)	0.156 5(3)
C(15)	0.432 4(2)	0.537 0(2)	0.027 7(4)	0.464 3(2)	0.008 2(2)	0.153 2(3)
C(16)	0.256 1(2)	0.476 3(2)	−0.009 7(4)	0.258 3(2)	0.026 5(2)	−0.010 3(3)
C(17)	0.368 8(2)	0.357 2(2)	−0.053 7(3)	0.366 6(2)	0.143 7(1)	−0.050 1(3)
C(18)	0.398 5(2)	0.345 2(2)	−0.120 4(3)	0.395 5(2)	0.157 5(2)	−0.118 2(3)
C(19)	0.443 3(2)	0.326 4(2)	−0.102 7(3)	0.441 9(2)	0.175 2(2)	−0.102 0(3)
C(20)	0.457 0(2)	0.321 1(2)	−0.020 3(3)	0.457 6(2)	0.179 3(2)	−0.017 5(3)
C(21)	0.425 9(2)	0.334 5(2)	0.046 8(3)	0.426 8(2)	0.164 1(1)	0.049 1(3)
C(22)	0.439 5(2)	0.329 3(2)	0.137 4(3)	0.441 2(2)	0.166 6(2)	0.142 1(3)
C(23)	0.403 8(2)	0.332 3(2)	0.277 1(3)	0.402 9(1)	0.165 3(1)	0.281 7(3)
C(24)	0.367 5(2)	0.344 0(2)	0.337 4(3)	0.364 8(2)	0.153 2(2)	0.339 9(3)
C(25)	0.326 9(2)	0.369 9(2)	0.322 3(3)	0.324 0(1)	0.125 9(1)	0.320 6(3)
C(26)	0.291 4(2)	0.379 1(2)	0.390 9(3)	0.286 9(2)	0.116 1(1)	0.389 2(3)
C(27)	0.305 0(2)	0.381 3(2)	0.477 7(3)	0.238 3(2)	0.110 8(1)	0.367 3(3)
C(28)	0.270 7(2)	0.386 7(2)	0.539 5(4)	0.201 9(2)	0.106 0(2)	0.430 4(3)
C(29)	0.223 3(2)	0.390 8(2)	0.519 9(4)	0.215 4(2)	0.105 5(2)	0.517 3(3)
C(30)	0.209 8(2)	0.390 2(2)	0.436 7(4)	0.263 9(2)	0.108 9(2)	0.539 9(3)
C(31)	0.243 9(2)	0.385 4(2)	0.370 8(3)	0.299 6(2)	0.114 8(2)	0.477 8(3)
C(32)	0.449 3(2)	0.311 1(2)	0.313 0(4)	0.449 0(2)	0.185 0(2)	0.319 0(3)

* Data for the anion have been deposited.

characterize the electronic spin state and properties of the spin-crossover behaviour; representative spectra are shown in Fig. 2 and Mössbauer parameters are listed in Table 4. The spectra at 330 and 78 K are typical of those for high- and low-spin iron(III), respectively. The quadrupole splitting for the low-spin state, 1.48 mm s^{-1}, is less than that for $[Fe(acpa)_2]PF_6$ (2.23 mm s^{-1});[27] the decrease seems to result from the change in q_{val} (the electric field gradient due to lattice contribution) because the iron atoms have a distorted octahedral co-ordination in both cases.

The temperature dependence of the relative absorption area under the Mössbauer resonance curve is plotted in Fig. 3, where $A(T)$ is the area at temperature T. The plot is curved owing to the difference in the recoilless fraction between the high- and low-spin forms, and is consistent with the fact that an abrupt phase transition does not occur in the temperature range employed in this work. Thus the rearrangement of the co-ordination sphere of the complex would occur continuously and demand a very small change in geometry.

The quadrupole splitting of low-spin iron(III) is sensitive to a change in temperature if the first excited state of the d orbitals is separated from the ground state by an energy of the order of the thermal energy kT. The decrease in quadrupole splitting at 148 K relative to that at 78 K is small for the bzpa complexes, and so it is not anticipated that the values decrease abruptly above 148 K. Therefore, the decrease in quadrupole splitting above 148 K is due to the rapid electronic spin-state interexchange.

Our best fits are illustrated in Fig. 2. Fitting was tried in the transition temperature range. The relaxation time τ is represented by $\tau = \tau_{ls}\tau_{hs}/(\tau_{ls} + \tau_{hs})$, where τ_{hs} and τ_{ls} are the lifetimes of the high- and low-spin isomers, respectively. The observed spectra are the result of rapid relaxation on the Mössbauer time-scale of 10^{-8} s between high- and low-spin states. A fitting should involve computing a distribution of relaxation spectra, correction for the line broadening resulting from the thick absorber and the temperature dependence of the quadrupole splitting for the low-spin isomer. Such a complex treatment was not attempted and consequently the absolute values of the relaxation rate should be taken with caution. The rates for the forward (k_1) and reverse (k_{-1}) rate constants for the spin interconversion $^2T_2 \rightleftharpoons {}^6A_1$ are defined at $1/\tau_{ls}$ and $1/\tau_{hs}$, respectively. The relations $f_{hs} + f_{ls} = 1$ and $k_1 f_{ls} = k_{-1} f_{hs}$ are fulfilled, where f_{hs} and f_{ls} are the fractions of the high- and low-spin forms. A plot of the natural logarithm of the equilibrium constant $K = k_1/k_{-1}$ *vs.* $1/T$ in the temperature region where both spin states are present in appreciable amounts yields an enthalpy change of 28 kJ mol^{-1} (=2400 cm^{-1}), which is larger than 840 cm^{-1} for $[Fe(acpa)_2]BPh_4$[27] and 1700 cm^{-1} for $[Fe\{HB(pz)_3\}_2]$.[32]

Mössbauer spectra for the acen complex were reported in the early work.[13] The sample obtained in this work shows similar

Table 3 Positional parameters for $[Fe(acen)(NC_5H_3Me_2\text{-}3,4)_2]BPh_4$*

	At 290 K			At 120 K		
Atom	*x*	*y*	*z*	*x*	*y*	*z*
Fe	0.115 88(2)	0.010 45(4)	0.199 54(5)	0.119 88(1)	0.009 46(2)	0.192 70(3)
O(1)	0.071 9(1)	0.047 0(2)	0.073 4(2)	0.071 5(1)	0.050 0(1)	0.079 0(1)
O(2)	0.077 0(1)	0.031 9(2)	0.338 2(2)	0.074 8(1)	0.036 6(1)	0.317 0(1)
N(1)	0.168 2(1)	−0.006 7(2)	0.073 6(3)	0.167 8(1)	−0.006 2(1)	0.070 9(2)
N(2)	0.168 7(1)	−0.042 6(2)	0.309 6(3)	0.167 3(1)	−0.041 2(1)	0.304 1(2)
N(P1)	0.138 5(1)	0.155 9(2)	0.221 5(3)	0.142 2(1)	0.146 0(1)	0.217 6(2)
N(P2)	0.088 0(1)	−0.130 9(2)	0.177 0(3)	0.093 1(1)	−0.123 9(1)	0.169 8(2)
C(1)	0.078 3(2)	0.053 9(3)	−0.040 7(4)	0.075 7(1)	0.055 0(2)	−0.037 4(2)
C(2)	0.121 0(2)	0.038 6(3)	−0.095 9(4)	0.118 1(1)	0.039 6(2)	−0.099 1(2)
C(3)	0.164 0(1)	0.011 4(3)	−0.041 6(3)	0.163 0(1)	0.012 8(2)	−0.046 4(2)
C(4)	0.214 4(1)	−0.029 0(3)	0.128 2(4)	0.215 7(1)	−0.027 9(2)	0.124 5(2)
C(5)	0.207 0(2)	−0.085 2(3)	0.240 7(4)	0.207 8(1)	−0.084 7(2)	0.239 4(2)
C(6)	0.167 2(1)	−0.051 0(3)	0.426 5(4)	0.163 4(1)	−0.050 9(2)	0.423 1(2)
C(7)	0.130 2(2)	−0.011 6(3)	0.493 7(3)	0.123 8(1)	−0.010 8(2)	0.485 3(2)
C(8)	0.089 2(2)	0.029 1(3)	0.450 6(4)	0.084 2(1)	0.033 2(2)	0.432 3(2)
C(9)	0.034 8(2)	0.081 2(4)	−0.111 0(4)	0.030 4(1)	0.081 8(2)	−0.106 2(2)
C(10)	0.207 1(2)	0.004 4(3)	−0.122 0(4)	0.205 2(1)	0.004 3(2)	−0.129 8(2)
C(11)	0.206 4(2)	−0.101 8(3)	0.495 0(4)	0.201 4(1)	−0.102 3(2)	0.497 7(2)
C(12)	0.054 6(2)	0.074 7(4)	0.534 9(4)	0.047 9(1)	0.083 1(2)	0.510 8(3)
C(P11)	0.122 6(2)	0.222 5(3)	0.146 8(4)	0.128 2(1)	0.214 2(2)	0.139 5(2)
C(P12)	0.131 6(2)	0.317 6(3)	0.164 2(4)	0.135 9(1)	0.310 5(2)	0.158 8(2)
C(P13)	0.158 3(2)	0.344 1(3)	0.265 5(4)	0.159 1(1)	0.338 2(2)	0.267 5(2)
C(P14)	0.174 1(2)	0.274 7(3)	0.341 6(4)	0.174 4(1)	0.267 4(2)	0.346 0(2)
C(P15)	0.163 5(1)	0.183 2(3)	0.316 9(4)	0.165 3(1)	0.173 9(2)	0.319 3(2)
C(P16)	0.111 4(2)	0.385 7(4)	0.074 4(5)	0.118 9(1)	0.380 9(2)	0.065 2(3)
C(P17)	0.169 6(2)	0.444 8(3)	0.291 0(5)	0.167 8(1)	0.441 3(2)	0.295 6(3)
C(P21)	0.066 5(1)	−0.176 2(3)	0.267 2(4)	0.070 2(1)	−0.168 7(2)	0.259 7(2)
C(P22)	0.043 1(1)	−0.261 6(3)	0.252 5(4)	0.046 6(1)	−0.254 9(2)	0.246 6(2)
C(P23)	0.042 7(2)	−0.301 9(3)	0.138 7(4)	0.046 6(1)	−0.298 2(2)	0.131 3(2)
C(P24)	0.065 5(2)	−0.256 2(3)	0.047 4(4)	0.070 6(1)	−0.253 0(2)	0.038 8(2)
C(P25)	0.087 9(2)	−0.172 2(3)	0.069 4(4)	0.093 2(1)	−0.167 3(2)	0.059 6(2)
C(P26)	0.019 2(2)	−0.305 9(4)	0.357 5(5)	0.020 7(1)	−0.298 1(2)	0.351 7(3)
C(P27)	0.016 4(2)	−0.393 5(4)	0.113 5(5)	0.020 9(1)	−0.391 1(2)	0.109 3(3)

* Data for the anion have been deposited.

Table 4 Mössbauer parameters of $[Fe(bzpa)_2]ClO_4$ at various temperatures

	δ_{Fe}[a]	ΔE[b]	Γ_l[c]	Γ_h[d]		
T/K	mm s^{-1}				ln[*A*(*T*)/*A*(100)]	χ[e]
78	0.190	1.485	0.326	0.304	0.150	462
100	0.189	1.452	0.308	0.291	0.000	552
123	0.184	1.432	0.299	0.290	−0.086	465
148	0.175	1.396	0.287	0.282	−0.276	484
170	0.171	1.363	0.332	0.332	−0.413	519
203	0.167	1.300	0.443	0.446	−0.571	452
232	0.189	1.151	0.572	0.697	−0.754	468
251	0.209	1.016	0.696	0.807	−0.944	499
270	0.217	0.878	0.780	0.912	−1.094	461
288	0.177	0.743	0.659	1.041	−1.315	486
319	0.178	0.590	0.651	1.001	−1.580	457
330	0.159	0.621	0.858	0.956	−1.708	416

[a] Isomer shift. [b] Quadrupole splitting. [c] Full width at half maximum (f.w.h.m.) for low-energy line. [d] f.w.h.m. for high-energy line. [e] Sum of the squares of the weighted residuals (relative to 493).

behaviour without observable crystal-packing effects: in the spin-crossover range, superposition of the two doublets of the high- and low-spin forms is observed.

Molecular and Crystal structure of $[Fe(bzpa)_2]ClO_4$.—The molecular structure of the bzpa complex was determined at 290 (high-spin state) and at 140 K (low-spin state). A perspective drawing of the $[Fe(bzpa)_2]^+$ cation at 140 K is illustrated in Fig. 4. The complex has a very similar structure at 290 K which is therefore not shown. The bond lengths and angles are contained in Tables 5 and 6. The ClO_4^- ion was found to be disordered in two positions about one Cl–O axis and having equal occupancy within experimental error. Since the complex cation is well defined, and the ClO_4^- ion not of primary interest, this disorder problem was not pursued further.

The environment of the cation is comprised of N_4O_2 donors from the two bzpa moieties and a pseudo-octahedral co-ordination with *cis* geometry for the two oxygen atoms. The angles O(1)–Fe–N(1) 168.2° and O(2)–Fe–N(3) 168.9° markedly deviate from those for an ideal octahedron (180°), but approach the ideal angles, 174.5 and 176.2°, at 140 K mainly due to the displacement of atoms O(1) and O(2) because the angles Fe–O(1)–C(9) and Fe–O(2)–C(25) change markedly with spin-state transformation.

The molecule has no crystallographically imposed symmetry, and deviates significantly from the idealized two-fold rotation symmetry. The average Fe–O[O(1) or O(2)] bond distance associated with the benzoylacetone residue is the shortest (1.921 Å at 290 K, 1.908 Å at 140 K). The average pyridine Fe–N[N(1) and N(3)] bond length (2.074–1.976 Å) is longer than the average imine Fe–N[N(2) and N(4)] (2.017–1.920 Å). The average iron–donor atom distances are in accord with values reported for other Schiff base–iron(III) complexes with N_4O_2 donors. The average change in Fe–L bond length between the high- and low-spin forms is 0.069 Å, the smallest value so far reported.

Crystal and Molecular Structure of $[Fe(acen)(NC_5H_3Me_2\text{-}3,4)_2]BPh_4$.—A perspective drawing of the $[Fe(acen)(NC_5H_3Me_2\text{-}3,4)_2]^+$ cation at 120 K with the numbering scheme is illustrated in Fig. 5. The bond lengths and angles are

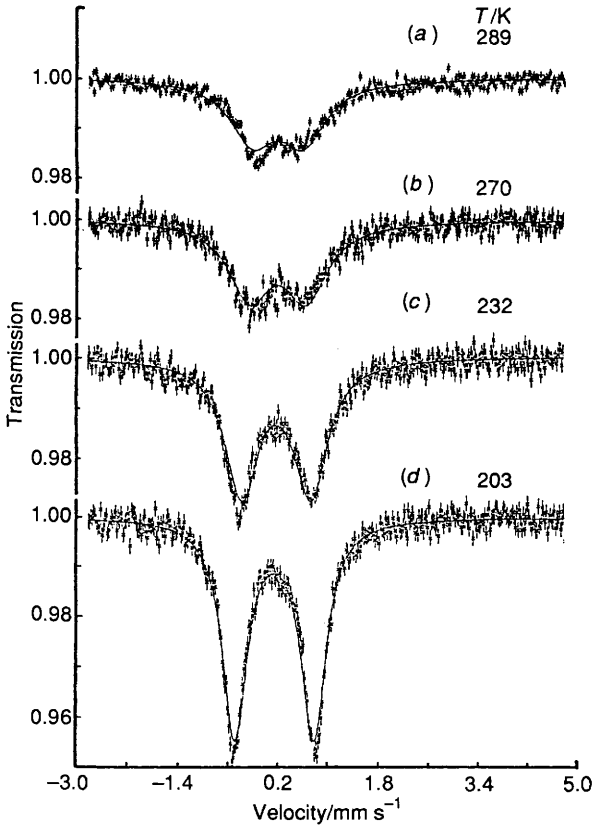

Fig. 2 Representative Mössbauer spectra for $[Fe(bzpa)_2]ClO_4$ at various temperatures and attempt to obtain a best fit between the Mössbauer spectra for $[Fe(bzpa)_2]ClO_4$ and the model. The full curves are calculated by using the following parameters: (*a*) $f_{hs} = 0.63$, $\Gamma = 0.860$ mm s^{-1}, $\tau = 0.25 \times 10^{-7}$ s; (*b*) $f_{hs} = 0.53$, $\Gamma = 0.574$ mm s^{-1}, $\tau = 0.47 \times 10^{-7}$ s; (*c*) $f_{hs} = 0.32$, $\Gamma = 0.427$ mm s^{-1}, $\tau = 0.86 \times 10^{-7}$ s; (*d*) $f_{hs} = 0.16$, $\Gamma = 0.768$ mm s^{-1}, $\tau = 0.14 \times 10^{-6}$ s

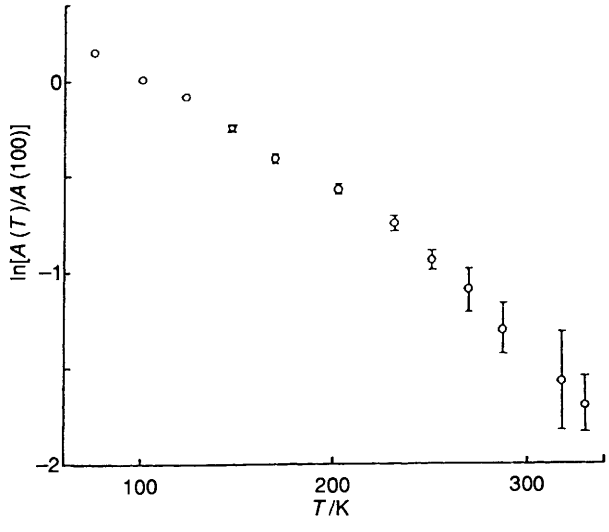

Fig. 3 Temperature dependence of $\ln[A(T)/A(100)]$ for $[Fe(bzpa)_2]ClO_4$

summarized in Tables 7 and 8, respectively. The environment of the cation is comprised of N_4O_2 donors and a pseudo-octahedral co-ordination with *cis* geometry for the two oxygen atoms. The basal plane comprises the N_2O_2 donors of the acen moiety and forms a slight tetrahedral distortion. A deviation from the octahedral symmetry of the FeN_4O_2 unit is indicated by the bond lengths and angles. The angles N(P1)–Fe–O(1) 90.3, N(P1)–Fe–N(1) 89.0, N(P1)–Fe–O(2) 85.7 and N(P1)–Fe–N(2) 94.5° are distorted from that for a ideal

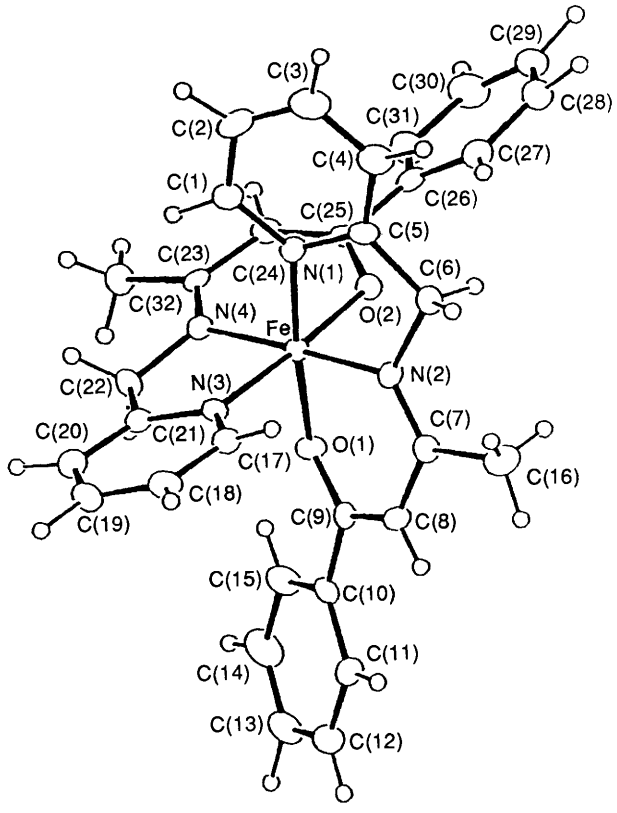

Fig. 4 Perspective drawing for $[Fe(bzpa)_2]^+$ at 140 K

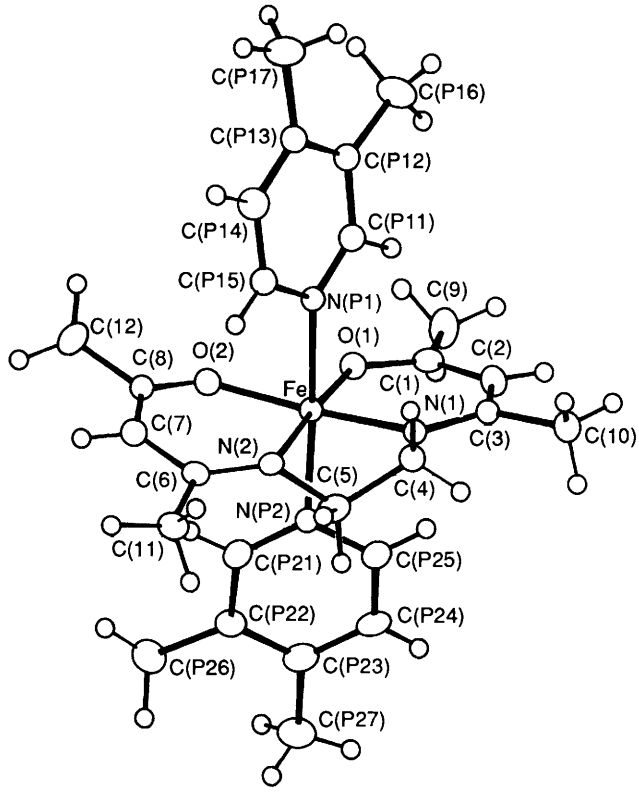

Fig. 5 Perspective drawing for $[Fe(acen)(NC_5H_3Me_2\text{-}3,4)_2]^+$ at 120 K

octahedron (90°), and the changes in these angles between the high-and low-spin form are less than 1°. The two axial positions are occupied by the nitrogen atom of the 3,4-dimethylpyridine and the angle N(P1)–Fe–N(P2) is about 176° and does not change with spin-state transformation. However, the angles O(2)–Fe–N(1) 168.9 and O(1)–Fe–N(2) 169.4° at 290

Table 5 Bond lengths (Å) for $[Fe(bzpa)_2]^+$ with estimated standard deviations in parentheses

	At 290 K	At 140 K		At 290 K	At 140 K
Fe–O(1)	1.911(3)	1.896(3)	Fe–O(2)	1.930(3)	1.919(3)
Fe–N(1)	2.070(4)	1.964(3)	Fe–N(2)	2.018(4)	1.914(3)
Fe–N(3)	2.078(4)	1.988(3)	Fe–N(4)	2.015(4)	1.926(3)
N(1)–C(1)	1.336(6)	1.352(5)	N(3)–C(17)	1.363(6)	1.355(5)
C(1)–C(2)	1.364(8)	1.378(6)	C(17)–C(18)	1.367(7)	1.369(6)
C(2)–C(3)	1.368(10)	1.373(7)	C(18)–C(19)	1.388(8)	1.386(6)
C(3)–C(4)	1.376(9)	1.392(7)	C(19)–C(20)	1.342(8)	1.376(6)
C(4)–C(5)	1.376(7)	1.387(6)	C(20)–C(21)	1.406(7)	1.393(6)
C(5)–C(6)	1.498(7)	1.500(6)	C(21)–C(22)	1.464(7)	1.487(6)
C(5)–N(1)	1.332(6)	1.342(5)	C(21)–N(3)	1.328(6)	1.348(5)
C(6)–N(2)	1.478(6)	1.471(5)	C(22)–N(4)	1.470(6)	1.465(5)
N(2)–C(7)	1.306(6)	1.318(5)	N(4)–C(23)	1.308(6)	1.321(5)
C(7)–C(16)	1.504(7)	1.504(6)	C(23)–C(32)	1.510(7)	1.491(6)
C(7)–C(8)	1.421(7)	1.414(6)	C(23)–C(24)	1.419(7)	1.418(6)
C(8)–C(9)	1.363(6)	1.385(6)	C(24)–C(25)	1.366(6)	1.381(6)
C(9)–O(1)	1.303(5)	1.294(5)	C(25)–O(2)	1.302(5)	1.300(5)
C(9)–C(10)	1.481(6)	1.491(6)	C(25)–C(26)	1.478(6)	1.492(6)
C(10)–C(11)	1.396(7)	1.397(6)	C(26)–C(27)	1.401(7)	1.385(6)
C(11)–C(12)	1.377(8)	1.375(6)	C(27)–C(28)	1.364(8)	1.398(6)
C(12)–C(13)	1.378(10)	1.376(7)	C(28)–C(29)	1.367(9)	1.388(7)
C(13)–C(14)	1.355(9)	1.369(7)	C(29)–C(30)	1.345(9)	1.381(7)
C(14)–C(15)	1.367(8)	1.387(7)	C(30)–C(31)	1.406(8)	1.378(7)
C(15)–C(10)	1.366(7)	1.394(6)	C(31)–C(26)	1.377(7)	1.408(6)

Table 6 Bond angles (°) for $[Fe(bzpa)_2]^+$ with estimated standard deviations in parentheses

	At 290 K	At 140 K		At 290 K	At 140 K
O(1)–Fe–O(2)	95.4(1)	92.2(1)	O(1)–Fe–N(1)	168.2(1)	174.5(1)
O(1)–Fe–N(2)	89.1(1)	92.3(1)	O(1)–Fe–N(3)	89.4(1)	88.9(1)
O(1)–Fe–N(4)	90.2(1)	86.8(1)	O(2)–Fe–N(1)	86.5(1)	85.9(1)
O(2)–Fe–N(2)	91.7(1)	87.9(1)	O(2)–Fe–N(3)	168.9(1)	176.2(1)
O(2)–Fe–N(4)	90.4(1)	93.7(1)	N(1)–Fe–N(2)	79.2(1)	82.6(1)
N(1)–Fe–N(3)	90.8(2)	93.3(1)	N(1)–Fe–N(4)	101.5(1)	98.4(1)
N(2)–Fe–N(3)	98.4(1)	95.7(1)	N(2)–Fe–N(4)	177.8(1)	178.2(1)
N(3)–Fe–N(4)	79.6(1)	82.7(1)			
Fe–N(1)–C(1)	125.6(4)	126.1(3)	Fe–N(3)–C(17)	125.8(3)	127.5(3)
Fe–N(1)–C(5)	113.9(3)	113.8(3)	Fe–N(3)–C(21)	114.9(3)	114.3(3)
C(1)–N(1)–C(5)	119.6(4)	120.0(4)	C(17)–N(3)–C(21)	119.2(4)	118.3(3)
N(1)–C(1)–C(2)	121.4(5)	120.3(4)	N(3)–C(17)–C(18)	121.3(5)	122.1(4)
C(1)–C(2)–C(3)	119.4(5)	120.5(4)	C(17)–C(18)–C(19)	119.4(5)	119.5(4)
C(2)–C(3)–C(4)	119.4(6)	119.0(4)	C(18)–C(19)–C(20)	119.2(5)	119.2(4)
C(3)–C(4)–C(5)	118.6(5)	118.5(4)	C(19)–C(20)–C(21)	120.0(5)	118.8(4)
C(4)–C(5)–C(6)	121.1(4)	122.7(4)	C(20)–C(21)–C(22)	121.7(4)	122.3(4)
C(4)–C(5)–N(1)	121.5(5)	121.6(4)	C(20)–C(21)–N(3)	120.8(4)	122.1(4)
N(1)–C(5)–C(6)	117.4(4)	115.7(4)	N(3)–C(21)–C(22)	117.6(4)	115.6(4)
C(5)–C(6)–N(2)	109.1(4)	108.2(3)	C(21)–C(22)–N(4)	111.1(4)	109.8(3)
Fe–N(2)–C(7)	126.2(3)	126.0(3)	Fe–N(4)–C(23)	126.5(3)	126.7(3)
C(6)–N(2)–C(7)	120.1(4)	120.6(3)	C(22)–N(4)–C(23)	118.6(4)	118.3(3)
Fe–N(2)–C(6)	113.5(3)	113.0(3)	Fe–N(4)–C(22)	114.3(3)	113.6(3)
N(2)–C(7)–C(16)	121.3(4)	120.5(4)	N(4)–C(23)–C(32)	120.9(4)	120.7(4)
N(2)–C(7)–C(8)	121.2(4)	121.1(4)	N(4)–C(23)–C(24)	122.4(4)	121.4(4)
C(8)–C(7)–C(16)	117.5(4)	118.3(4)	C(24)–C(23)–C(32)	116.7(4)	117.8(4)
C(7)–C(8)–C(9)	127.5(4)	125.8(4)	C(23)–C(24)–C(25)	127.2(4)	126.1(4)
Fe–O(1)–C(9)	127.9(3)	125.0(3)	Fe–O(2)–C(25)	129.0(3)	124.6(3)
O(1)–C(9)–C(8)	122.0(4)	122.9(4)	O(2)–C(25)–C(24)	123.5(4)	125.3(4)
O(1)–C(9)–C(10)	114.8(4)	114.5(3)	O(2)–C(25)–C(26)	114.7(4)	114.8(4)
C(8)–C(9)–C(10)	123.0(4)	122.6(4)	C(24)–C(25)–C(26)	121.8(4)	120.0(4)
C(9)–C(10)–C(11)	118.7(4)	123.5(4)	C(25)–C(26)–C(27)	121.2(4)	120.3(4)
C(9)–C(10)–C(15)	125.1(4)	118.8(4)	C(25)–C(26)–C(31)	120.5(4)	121.5(4)
C(11)–C(10)–C(15)	116.1(5)	117.7(4)	C(27)–C(26)–C(31)	118.3(5)	118.1(4)
C(10)–C(11)–C(12)	122.3(5)	120.7(4)	C(26)–C(27)–C(28)	119.5(5)	121.9(4)
C(11)–C(12)–C(13)	118.4(6)	120.8(4)	C(27)–C(28)–C(29)	122.3(6)	118.8(4)
C(12)–C(13)–C(14)	120.7(6)	119.8(4)	C(28)–C(29)–C(30)	119.1(6)	119.9(4)
C(13)–C(14)–C(15)	119.6(6)	120.1(4)	C(29)–C(30)–C(31)	120.6(5)	121.2(4)
C(14)–C(15)–C(10)	122.9(5)	121.0(4)	C(30)–C(31)–C(26)	120.2(5)	120.1(4)

K increase to 174.6 and 175.6° at 120 K, respectively. A remarkable decrease in the angle O(1)–Fe–O(2) in the basal plane is observed with spin-state transformation (from 100.4 to 87.0°), and so other angles O(1)–Fe–N(1), N(1)–Fe–N(2) and N(2)–Fe–O(2) in the basal plane become large. The Fe–O bond distances associated with the acen residue are the shortest (average 1.930 Å at 290 K, 1.906 Å at 120 K) followed by those to the imine Fe–N(1) [or N(2)] (average 2.058–1.918 Å) and to the 3,4-dimethylpyridine Fe-N(P1) [or N(P2)] (average 2.186–2.036 Å). The average change in Fe–L(L = co-ordinated atom)

Table 7 Bond lengths (Å) for $[Fe(acen)(NC_5H_3Me_2\text{-}3,4)_2]^+$ with estimated standard deviations in parentheses

	At 290 K	At 120 K		At 290 K	At 120 K
Fe–O(1)	1.932(3)	1.905(2)	Fe–O(2)	1.927(3)	1.907(2)
Fe–N(1)	2.058(3)	1.916(2)	Fe–N(2)	2.057(3)	1.919(2)
Fe–N(P1)	2.190(3)	2.037(2)	Fe–N(P2)	2.182(3)	2.034(2)
O(1)–C(1)	1.292(5)	1.290(3)	C(1)–C(9)	1.493(7)	1.502(4)
C(1)–C(2)	1.369(6)	1.384(4)	C(2)–C(3)	1.399(6)	1.414(3)
C(3)–C(10)	1.518(6)	1.503(3)	C(3)–N(1)	1.316(5)	1.322(3)
N(1)–C(4)	1.458(5)	1.473(3)	C(4)–C(5)	1.508(6)	1.515(3)
C(5)–N(2)	1.462(5)	1.471(3)	N(2)–C(6)	1.312(5)	1.323(3)
C(6)–C(11)	1.516(6)	1.507(4)	C(6)–C(7)	1.405(6)	1.421(4)
C(7)–C(8)	1.371(6)	1.380(4)	C(8)–C(12)	1.507(7)	1.510(4)
C(8)–O(2)	1.297(5)	1.292(3)	N(P1)–C(P11)	1.340(5)	1.341(3)
C(P11)–C(P12)	1.396(6)	1.388(4)	C(P12)–C(P16)	1.504(7)	1.498(4)
C(P12)–C(P13)	1.401(6)	1.403(4)	C(P13)–C(P17)	1.501(6)	1.502(4)
C(P13)–C(P14)	1.378(6)	1.381(4)	C(P14)–C(P15)	1.371(6)	1.371(4)
C(P15)–N(P1)	1.325(5)	1.339(3)	N(P2)–C(P21)	1.346(5)	1.342(3)
C(P21)–C(P22)	1.397(6)	1.386(4)	C(P22)–C(P26)	1.498(7)	1.501(4)
C(P22)–C(P23)	1.395(6)	1.407(4)	C(P23)–C(P27)	1.529(7)	1.507(4)
C(P23)–C(P24)	1.375(6)	1.382(4)	C(P24)–C(P25)	1.377(6)	1.376(4)
C(P25)–N(P2)	1.338(5)	1.358(3)			

Table 8 Bond Angles (°) for $[Fe(acen)(NC_5H_3Me_2\text{-}3,4)_2]^+$ with estimated standard deviations in parentheses

	At 290 K	At 120 K		At 290 K	At 120 K
O(1)–Fe–O(2)	100.4(1)	87.0(1)	O(1)–Fe–N(1)	89.3(1)	93.7(1)
O(1)–Fe–N(2)	169.4(1)	175.6(1)	O(1)–Fe–N(P1)	90.3(1)	90.8(1)
O(1)–Fe–N(P2)	86.7(1)	86.8(1)	O(2)–Fe–N(1)	168.9(1)	174.6(1)
O(2)–Fe–N(2)	89.3(1)	93.9(1)	O(2)–Fe–N(P1)	85.7(1)	85.2(1)
O(2)–Fe–N(P2)	92.0(1)	91.8(1)	N(1)–Fe–N(2)	81.4(1)	85.9(1)
N(1)–Fe–N(P1)	89.0(1)	89.4(1)	N(1)–Fe–N(P2)	93.9(1)	93.6(1)
N(2)–Fe–N(P1)	94.5(1)	93.6(1)	N(2)–Fe–N(P2)	88.9(1)	88.9(1)
N(P1)–Fe–N(P2)	175.9(1)	176.2(1)			
Fe–O(1)–C(1)	130.2(3)	126.4(2)	Fe–O(2)–C(8)	128.9(3)	125.0(2)
O(1)–C(1)–C(2)	124.3(4)	124.8(2)	O(1)–C(1)–C(9)	114.6(4)	115.1(2)
C(9)–C(1)–C(2)	121.1(4)	120.1(2)	C(1)–C(2)–C(3)	127.0(4)	126.2(2)
C(2)–C(3)–N(1)	123.1(4)	121.8(2)	C(2)–C(3)–C(10)	116.8(4)	117.4(2)
N(1)–C(3)–C(10)	120.2(4)	120.9(2)	Fe–N(1)–C(3)	126.0(3)	126.9(2)
Fe–N(1)–C(4)	112.1(2)	112.0(1)	C(3)–N(1)–C(4)	121.4(3)	120.5(2)
N(1)–C(4)–C(5)	109.6(3)	107.5(2)	C(4)–C(5)–N(2)	109.0(3)	107.9(2)
Fe–N(2)–C(5)	111.5(2)	111.4(2)	C(5)–N(2)–C(6)	121.2(3)	120.8(2)
Fe–N(2)–C(6)	126.7(3)	127.1(2)	N(2)–C(6)–C(11)	121.0(4)	121.3(2)
C(11)–C(6)–C(7)	117.3(4)	117.9(2)	N(2)–C(6)–C(7)	121.7(4)	120.9(2)
C(6)–C(7)–C(8)	127.2(4)	126.3(2)	C(7)–C(8)–O(2)	124.2(4)	125.2(2)
C(7)–C(8)–C(12)	120.5(4)	120.1(2)	C(12)–C(8)–O(2)	115.4(4)	114.8(2)
C(8)–O(2)–Fe	128.9(3)	125.0(2)	Fe–N(P1)–C(P11)	120.8(3)	120.5(2)
Fe–N(P1)–C(P15)	121.3(3)	122.0(2)	C(P11)–N(P1)–C(P15)	117.4(3)	117.0(2)
N(P1)–C(P11)–C(P12)	123.2(4)	124.1(2)	C(P11)–C(P12)–C(P13)	118.1(4)	118.0(2)
C(P11)–C(P12)–C(P16)	118.2(4)	119.8(3)	C(P16)–C(P12)–C(P13)	123.7(4)	122.3(2)
C(P12)–C(P13)–C(P14)	117.8(4)	117.5(2)	C(P12)–C(P13)–C(P17)	121.6(4)	120.9(2)
C(P17)–C(P13)–C(P14)	120.6(4)	121.5(3)	C(P13)–C(P14)–C(P15)	119.8(4)	120.4(2)
C(P14)–C(P15)–N(P1)	123.7(4)	123.0(2)	Fe–N(P2)–C(P21)	121.5(3)	121.2(2)
Fe–N(P2)–C(P25)	120.6(3)	121.3(2)	C(P21)–N(P2)–C(P25)	117.6(3)	117.1(2)
N(P2)–C(P21)–C(P22)	123.2(4)	124.3(2)	C(P21)–C(P22)–C(P23)	117.9(4)	117.8(2)
C(P21)–C(P22)–C(P26)	119.5(4)	120.4(2)	C(P26)–C(P22)–C(P23)	122.6(4)	121.7(2)
C(P22)–C(P23)–C(P24)	118.7(4)	118.1(2)	C(P22)–C(P23)–C(P27)	121.4(4)	120.9(2)
C(P27)–C(P23)–C(P24)	119.9(4)	121.0(3)	C(P23)–C(P24)–C(P25)	119.9(4)	120.4(2)
C(P24)–C(P25)–N(P2)	122.8(4)	122.3(2)			

in the high-spin form is 0.104 Å longer than that in the low-spin form and such bonds are the most sensitive to spin-state transformation.

The Fe–L bond lengths and Fe–O–C angles in spin-crossover complexes with Schiff bases for which the structures were confirmed for both electronic forms are summarized in Table 9. The average difference in bond lengths between the high- and low-spin forms of the complexes listed is 0.098 Å. The average difference for the bzpa complex is the smallest at 0.069 Å, but the complex does not represent pure high- and low-spin extremes and therefore represents a lower limit. These differences for spin-crossover complexes are less than the 0.13 Å estimated using data for complexes which do not experience spin crossover.

The decrease in Fe–L from the high- to the low-spin form is not uniform: the change in Fe–O is smallest, and Fe–N(imine or pyridine) largest. The Fe–O–C angles for the complexes listed in Table 9 are more sensitive to spin-state transformation than are the Fe–N–C angles. The oxygen atoms of Schiff-bases acen, salen, acpa and bzpa are freer for fluctuation of the angle Fe–O–C than are the nitrogen atoms of Fe–N–C (N of pyridine). The torsion resulting from the change in Fe–L distance with spin-state transformation is expected to be relaxed by a change in the angle Fe–O–C.

Crystal data for the spin-crossover complexes so far studied by X-ray diffraction are summarized in Table 10. The average volume difference ΔV for type I is 36×10^{-3} nm^3 (corresponds

Table 9 Bond lengths (Å),[a] Fe–O–C angles (°) and the differences between high- and low-spin forms for some spin-crossover complexes with Schiff-base ligands

Complex[b]	Fe–N	Fe–N′	Fe–O	Fe–O–C	Δ(Fe–N)	Δ(Fe–N′)	Δ(Fe–O)	Δ(Fe–O–C)	Ref.
$[FeL^1_2]ClO_4·C_6H_6$	2.085	2.176	1.921	—	0.128	0.148	0.064		33
	(1.957)	(2.028)	(1.857)	(—)					
$[Fe(acpa)_2]PF_6$	2.081	2.153	1.939	129.4	0.140	0.164	0.050	4.9	34
	(1.941)	(1.989)	(1.889)	(124.5)					
$[Fe(acpa)_2]BPh_4$	2.055	2.087	1.917	129.2	0.118	0.106	0.017	3.8	*c*
	(1.937)	(1.981)	(1.900)	(125.4)					
$[Fe(bzpa)_2]ClO_4$	2.017	2.074	1.921	128.5	0.097	0.098	0.013	3.7	*d*
	(1.920)	(1.976)	(1.908)	(124.8)					
$[Fe(acen)(NC_5H_3Me_2\text{-}3,4)_2]BPh_4$	2.057	2.185	1.929	129.6	0.139	0.149	0.023	3.9	*d*
	(1.918)	(2.036)	(1.906)	(125.7)					
$[Fe(salen)(Him)_2]ClO_4$	2.067	2.146	1.901	129.4	0.154	0.154	−0.002	4.7	25
	(1.913)	(1.992)	(1.903)	(124.7)					
$[FeL^2_2]NO_3$[e]	1.982	2.121	1.896)	—	—	—	—		35
	(1.936)	(2.047)	(1.883)	(—)					

N is an imino nitrogen atom, N′ an amine, imidazole or pyridine nitrogen atom. Values for low-spin form are in parentheses. [a] Average Fe–L bond length is given for complex with two Fe–L bonds. [b] L^1 = Schiff base derived from 3-ethoxysalicylaldehyde and *N*-(3-aminopropyl)aziridine, L^2 = Schiff-base derived by condensation of *N*-benzylethylenediamine and 3-allylsalicylaldehyde. [c] H. Oshio, K. Toriumi, Y. Maeda and Y. Takashima, *Inorg. Chem.*, in the press. [d] This work. [e] High-spin population is expected to be 33% at room temperature.

Table 10 Crystal data for spin-crossover complexes of which the structures have been determined for the high- and low-spin states.

Complexes	Space group (Spin state)		V_{hs}[a]	Z[b]	ΔV[c]	$\Delta V'$[d]	T[e]/K	Ref.
(*a*) Type I (fast spin-state interexchange on Mössbauer time-scale)								
$[Fe(S_2CNEt_2)_3]$	$P2_1/c(\frac{1}{2})$	$C2/n(\frac{5}{2})$	2 368	4	26	4.4	79–297	36
$[FeL^1_2]ClO_4·C_6H_6$	$P2_1/c(\frac{1}{2})$	$C2/c(\frac{5}{2})$	3 596	4	56	6.2	128–300	33
$[Fe(acpa)_2]PF_6$	$P2/a(\frac{1}{2})$	$P2/a(\frac{5}{2})$	1 311	2	23	3.5	120–293	34
$[Fe(acpa)_2]BPh_4$	$P\bar{1}(\frac{1}{2})$	$P\bar{1}(\frac{5}{2})$	2 006	2	34	3.4	120–311	*f*
$[Fe(salen)(Him)_2]ClO_4$	$P2_12_12_1(\frac{1}{2})$	$P2_12_12_1(\frac{5}{2})$	2 407	4	29	4.8	120–295	25
$[Fe(oep)(NC_5H_4Cl\text{-}3)_2]ClO_4$	$P\bar{1}(\frac{1}{2})$	$P\bar{1}(\frac{5}{2})$	1 107	1	>53	>4.8	*g*	37
$[Fe(bzpa)_2]ClO_4$	$I4_1/a(\frac{1}{2})$	$I4_1/a(\frac{5}{2})$	12 141	16	33	4.4	140–290	*h*
(*b*) Type II (slow spin-state interexchange on Mössbauer time-scale)[i]								
$[Fe(bipy)_2(NCS)_2]$	*Pcnb*(0)	*Pcnb*(2)	2 190	4			*j*	38
$[FeCl_2(Ph_2PCH{=}CHPPh_2)_2]·2Me_2CO$	$P2_1/a(\frac{1}{2})$	$P2_1/a(\frac{3}{2})$	2 689	2	98	7.3	130–295	39
$[FeBr(L^3)]BPh_4·CH_2Cl_2$	$P\bar{1}(0)$	$P\bar{1}(1)$	3 150	2	67	4.3	150–293	40
$[Fe_3L^4_6(H_2O)_6][CF_3SO_3]_6$	$P3_1/c(0)$	$P\bar{3}_1/c(2)$	4 166	2	85	4.1	105–300	41
$[Fe(NC_5H_4CH_2NH_2\text{-}2)_3]Cl_2·EtOH$	$P2_1/c(0)$	$P2_1/c(2)$	2 485	4	35	5.6	90–293	42
$[Fe(NC_5H_4CH_2NH_2\text{-}2)_3]Cl_2·MeOH$	*Pbna*(0)	*Pbna*(2)	4 782	8	21	3.5	115–227	42
$[Fe(NC_5H_4CH_2NH_2\text{-}2)_3]Br_2·EtOH$	$P2_1/n(0)$	$P2_1/n(2)$	2 611	4	48	7.3	106–294	43
$[Fe(acen)(NC_5H_3Me_2\text{-}3,4)_2]BPh_4$	$P2_1/a(\frac{1}{2})$	$P2_1/a(\frac{5}{2})$	4 478	4	47	4.2	120–290	*h*

[a] Unit-cell volume for high-spin isomer ($\times 10^{-3}$ nm^3). [b] Number of molecules in unit cell. [c] Difference in the volume ($\times 10^{-3}$ nm^3) of a molecule between high- and low-spin isomers, $V_{hs} - V_{ls}$. [d] Specific volume difference between high- and low-spin isomers $\Delta V' = \Delta V·Z/V_{hs}$ ($\times 10^{-2}$). [e] Temperature at which crystal structure was determined. [f] H. Oshio, K. Toriumi, Y. Maeda and Y. Takashima, *Inorg. Chem.*, in the press. [g] Population of high-spin isomer relative to total isomers is not large even at high temperature (expected to be 55%). [h] This work. [i] bipy = 2,2′-bipyridyl; L^3 = 1,1,4,7,10,10-hexaphenyl-1,4,7,10-tetraphosphadecane, L^4 = 4-ethyl-1,2,4-triazole. [j] Data not given in the reference.

to 22 cm^3 mol^{-1}), being less than the 57 × 10^{-3} nm^3 (average) for type II. The small value for the compounds of type I is also reflected in specific volume difference ($\Delta V'$) of a molecule between the high- and low-spin forms, where specific volume difference is expressed by $\Delta V·Z/V_{hs}$. The complexes showing fast electronic interexchange according to Mössbauer spectra have small $\Delta V'$ except for $[FeL^1_2]ClO_4·C_6H_6$. However, the boundary between types I and II is ambiguous; the volume differences between the high- and low-spin states and the difference in activation energy for spin-state interexchange are not the only factors determining the rates. Ease of reorganization between the high- and low-spin states would also be important, and the radiationless non-adiabatic multiphonon process occurring between the high- and low-spin states should be taken into consideration.

From the measurement of the spin-state interexchange rate in solution, an important factor in determining the interexchange kinetics is the nature of reorganization of the primary coordination sphere accompanying the spin exchange. In addition to the influence on the spin-state transformation described above of intramolecular and structural features, intermolecular effects are also important as shown previously.[11,12,15,44]

Acknowledgements

We thank Professors S. Kida and H. Okawa of Kyushu University for help.

References

1 P. B. Merrithew and P. G. Rasmussen, *Inorg. Chem.*, 1972, **11**, 325; R. Rickards, C. E. Johnson and H. A. O. Hill, *J. Chem. Phys.*, 1968, **48**, 5231.
2 N. Matsumoto, S. Ohta, C. Yoshimura, A. Ohyoshi, S. Kohata, H. Okawa and Y. Maeda, *J. Chem. Soc., Dalton Trans.*, 1985, 2575.
3 G. R. Hall and D. N. Hendrickson, *Inorg. Chem.*, 1976, **15**, 607.
4 K. R. Kunze, D. L. Perry and L. J. Wilson, *Inorg. Chem.*, 1977, **16**, 594.
5 V. V. Zelentsov, L. G. Bogdanova, A. V. Ablov, N. V. Gerbeleu, Ch. V. Dyatlova and J. Russian, *Inorg. Chem.*, 1973, **18**, 1410.

6 E. Sinn, G. Sim, E. V. Dose, M. F. Tweedle and L. J. Wilson, *J. Am. Chem. Soc.*, 1978, **100**, 3375.
7 Y. Maeda and Y. Takashima, *Comments Inorg. Chem.*, 1988, **7**, 41.
8 E. W. Müller, H. Spiering and P. Gütlich, *J. Chem. Phys.*,1983, **79**, 1439.
9 M. P. Edwards, C. D. Hoff, B. Curnutte, J. S. Eck and K. F. Purcell, *Inorg. Chem.*, 1984, **23**, 2613.
10 W. L. Driessen and P. H. van der Voort, *Inorg. Chim. Acta*, 1977, **21**, 217.
11 P. Gütlich, *Struct. Bonding (Berlin)*, 1981, **44**, 83.
12 W. D. Federer and D. N. Hendrickson, *Inorg. Chem.*, 1984, **23**, 3861, 3870.
13 H. Oshio, Y. Maeda and Y. Takashima, *Inorg. Chem.*, 1983, **22**, 2684; H. Oshio, K. Kitazaki, J. Mishiro, N. Kato, Y. Maeda and Y. Takashima, *J. Chem. Soc., Dalton Trans.*, 1987, 1341.
14 A. H. Ewald, R. L. Martin, E. Sinn and A. H. White, *Inorg. Chem.*, 1969, **8**, 1837.
15 M. Sorai and S. Seki, *J. Phys. Chem. Solids*, 1972, **33**, 575.
16 M. Sorai and S. Seki, *J. Phys. Chem. Solids*, 1974, **35**, 555.
17 M. Sorai, Y. Maeda and H. Oshio, *J. Phys. Chem. Solids*, 1990, **51**, 941.
18 N. Sasaki and T. Kambara, *J. Phys. Soc. Jpn.*, 1982, **51**, 1571.
19 T. Kambara, *J. Phys. Soc. Jpn.*, 1981, **50**, 2257.
20 W. G. Kiel, C. P. Köhler, H. Spiering and P. Gütlich, *Inorg. Chem.*, 1986, **25**, 1565.
21 E. Buhks, G. Navon, N. Bixon and J. Jortner, *J. Am. Chem. Soc.*, 1980, **102**, 2918.
22 M. D. Timken, A. M. Abdel-Mawgoud and D. N. Hendrickson, *Inorg. Chem.*, 1986, **25**, 160.
23 M. S. Haddad, M. W. Lynch, W. D. Federer and D. N. Hendrickson, *Inorg. Chem.*, 1981, **20**, 123.
24 Y. Nishida, S. Oshio and S. Kida, *Bull. Chem. Soc. Jpn.*, 1977, **50**, 119.
25 B. J. Kennedy, A. C. McGrath, K. S. Murray, B. W. Skelton and A. H. White, *Inorg. Chem.*, 1987, **26**, 483.
26 D. K. Geiger, Y. J. Lee and W. R. Scheidt, *J. Am. Chem. Soc.*, 1984, **106**, 6339; W. R. Scheidt, S. R. Osvath, Y. J. Lee, C. A. Reed, B. Schaevitz and G. P. Gupta, *Inorg. Chem.*, 1989, **28**, 1591.
27 Y. Maeda, N. Tsutsumi and Y. Takashima, *Inorg. Chem.*, 1984, **23**, 2440.
28 Y. Maeda, Y. Takashima, N. Matsumoto and A. Ohyoshi, *J. Chem. Soc., Dalton Trans.*, 1986, 1115.
29 *International Tables for X-Ray Crystallography*, Kynoch Press, Birmingham, 1974, vol. 4.
30 T. Sakurai and K. Kobayashi, *Sci. Rep. Inst. Chem. Phys. Res. (Jpn.)*, 1979, **55**, 69.
31 C. K. Johnson, ORTEP, Report ORNL-3794, Oak Ridge National Laboratory, Oak Ridge, TN, 1965.
32 F. Grandjean, G. J. Long, B. B. Hutchinson, La. Ohlhausen and P. Neill, *Inorg. Chem.*, 1989, **28**, 4406.
33 M. D. Timken, C. E. Strouse, S. M. Soltis, S. A. Daverio, D. N. Hendrickson, A. M. Abdel-Mawgoud and S. R. Wilson, *J. Am. Chem. Soc.*, 1986, **108**, 395.
34 Y. Maeda, H. Oshio, Y. Takashima, M. Mikuriya and M. Hidaka, *Inorg. Chem.*, 1986, **25**, 2958.
35 M. D. Timken, D. N. Hendrickson and E. Sinn, *Inorg. Chem.*, 1985, **24**, 3947.
36 J. G. Leipoldt and P. Coppens, *Inorg. Chem.*, 1973, **12**, 2269.
37 W. R. Sheidt, D. K. Geiger and K. J. Haller, *J. Am. Chem. Soc.*, 1982, **104**, 495.
38 E. König and K. Watson, *J. Chem. Phys. Lett.*, 1970, **6**, 457.
39 F. Cecconi, M. Di Vaira, S. Midollini, A. Orlandini and L. Sacconi, *Inorg. Chem.*, 1981, **20**, 3423.
40 M. Bacci and C. A. Ghilardi, *Inorg. Chem.*, 1974, **13**, 2398.
41 G. Vos, R. A. G. de Graaff, J. G. Haasnoot, A. M. van de Kraan, P. de Vaal and J. Reedijk, *Inorg. Chem.*, 1984, **23**, 2905.
42 B. A. Katz and C. E. Strouse, *J. Am. Chem. Soc.*, 1979, **101**, 6214; M. Mikami, M. Konno and Y. Saito, *Acta Crystallogr., Sect. B.*, 1980, **36**, 275.
43 A. M. Greenaway, C. J. O'Connor, A. Schrock and E. Sinn, *Inorg. Chem.*, 1979, **18**, 2692.
44 E. König, G. Ritter, S. K. Kulshreshtha and S. M. Nelson, *J. Am. Chem. Soc.*, 1983, **105**, 1924.

Received 5*th September* 1990; *Paper* 0/04048G